

First-principles molecular dynamics simulations at solid-liquid interfaces with a continuum solvent

Verónica M. Sánchez[†], Mariela Sued[‡], and Damián A. Scherlis[†]

[†]*Departamento de Química Inorgánica,*

Analítica y Química Física/INQUIMAE,

Facultad de Ciencias Exactas y Naturales,

Universidad de Buenos Aires, Ciudad Universitaria,

Pab. II, Buenos Aires (C1428EHA) Argentina and

[‡]*Instituto de Cálculo, Facultad de Ciencias Exactas y Naturales,*

Universidad de Buenos Aires, Ciudad Universitaria,

Pab. II, Buenos Aires (C1428EHA) Argentina

(Dated: November 11, 2021)

Abstract

Continuum solvent models have become a standard technique in the context of electronic structure calculations, yet, no implementations have been reported capable to perform molecular dynamics at solid-liquid interfaces. We propose here such a continuum approach in a DFT framework, using plane-waves basis sets and periodic boundary conditions. Our work stems from a recent model designed for Car-Parrinello simulations of quantum solutes in a dielectric medium [J. Chem. Phys. **124**, 74103 (2006)], for which the permittivity of the solvent is defined as a function of the electronic density of the solute. This strategy turns out to be inadequate for systems extended in two dimensions: the dependence of the dielectric function on the electronic density introduces a new term in the Kohn-Sham potential which becomes unphysically large at the interfacial region, seriously affecting the convergence of the self-consistent calculations. If the dielectric medium is properly redefined as a function of the atomic coordinates, a good convergence is obtained and the constant of motion is conserved during the molecular dynamics simulations. Moreover, a significant gain in efficiency can be achieved if the simulation box is partitioned in two, solving the Poisson problem separately for the “dry” region using fast Fourier transforms, and for the solvated or “wet” region using a multigrid method. Eventually both solutions are combined in a self-consistent procedure, and in this way Car-Parrinello molecular dynamics simulations of solid-liquid interfaces can be performed at a very moderate computational cost. This scheme is employed to investigate the acid-base equilibrium at the TiO₂-water interface. The aqueous behavior of titania surfaces has stimulated a large amount of experimental research, but many open questions remain concerning the molecular mechanisms determining the chemistry of the interface. Here we make an attempt to answer some of them, putting to the test our continuum model.

I. INTRODUCTION

The structure and the reactivity of solid surfaces have become major subjects of study in chemistry and condensed matter physics, and are at the core of much of the research conducted in materials science. In this context, electronic structure methods, in particular density functional theory (DFT) calculations, have played a fundamental role in the interpretation and the validation of the data coming from the different surface spectroscopies and microscopies, often providing new insights on top of those detaching from the available experimental techniques.¹ Throughout the past two decades a large number of DFT simulations has been reported on metallic and semiconducting surfaces, contributing precious information concerning atomic and electronic structure, thermodynamics, and reactivity.^{2–4} With very few exceptions, these simulations considered a slab in the gas phase. For a broad range of applications, however, the relevant phenomena occur in the presence of a liquid phase, as is often the case in processes related to electrochemistry and catalysis. The realization of liquid phase DFT simulations is therefore a much pursued objective—especially when many of the standard X-ray techniques like XPS or SAXS are unsuited to provide atomic scale information in solution—, but the inclusion of the solvent considerably increases the cost of first-principles calculations of periodic surfaces, and is therefore a rather uncommon practice.⁵

In an explicit solvation approach, the vacuum space in the simulation box is filled with solvent molecules. The subsequent growth in the size of the system is in part responsible for the increased computational expense, but, more importantly, there is the fact that a static picture is a very poor representation of the liquid state. Any solute admits a huge number of possible configurations for the solvent molecules around it, associated with multiple local

minima, the net solvation effect arising from a weighted average of all these.⁶ A geometry optimization would lead to a solid or glassy phase corresponding to one of these minima in the multidimensional potential energy surface, resulting in a dielectric screening typically different from the static limit observed in the liquid state. Hence, to capture the solvation effect, it is necessary to perform extensive statistical sampling involving either lengthy molecular dynamics or Monte-Carlo simulations. Alternatively, it is possible to resort to the so called continuum (or implicit solvent) models, in which the solvent molecules are replaced by a dielectric medium surrounding the solute and exhibiting the static screening of the solution.^{7,8} In this way, the polarization induced by the solvent is introduced in an averaged fashion, and the cost of the computation gets closer to the corresponding cost in vacuum by drastically reducing the number of degrees of freedom. On the other hand, the representation of the solvent structure is omitted, disregarding any possible solute-solvent specific interactions. Still, to overcome this problem, all or part of the first solvation shells can be included explicitly, with the dielectric medium extending beyond the limits of this cluster comprising the solute plus a few solvent molecules. In any case, the continuum model has a long tradition in quantum chemistry and has proved reliable and efficient to extract properties in solution of a large variety of molecular systems.⁶⁻⁹

In recent years a small number of implementations of the continuum model has been proposed in the context of density functional theory, plane-waves basis sets, and the Car-Parrinello method.¹⁰⁻¹³ To the best of our knowledge, none of them have been employed in molecular dynamics simulations of periodic surfaces.¹⁴ Here we revise the electrostatic continuum model of Fattebert and Gygi,^{11,13,15} proposing a new definition for the dielectric function to make the model suitable for the treatment of periodic slabs. The original formulation, in which the permittivity of the solvent is determined by the charge density of

the solute, has proved successful in the simulation of molecular and ionic solutes,^{11,13} and of extended systems like polymers, with periodicity in one dimension.¹⁶ In the case of solid surfaces, however, the convergence to the electronic ground state turns out to be impaired. In the sections that follow, we attribute this failure to a term in the Kohn-Sham potential originating in the dependence of the dielectric constant on the electronic density, and, to circumvent this issue, we redefine the permittivity as a function of the atomic positions. In this way the smooth electronic convergence is restored, along with a good conservation of the total energy in the molecular dynamics runs. The electrostatic problem in the presence of the dielectric medium is efficiently addressed with a multigrid method,^{17–19} which solves the Poisson equation in real space. Moreover, a significant increase in efficiency can be obtained if the simulation box is partitioned in two, solving the Poisson problem separately for the “dry” region using fast Fourier transforms, while restricting the multigrid treatment to the solvated or “wet” part of the supercell (and then combining both solutions in a self-consistent fashion). Using this scheme it is possible to carry out Car-Parrinello molecular dynamics simulations of solid-liquid interfaces at a computational cost exceeding by just a small factor the one corresponding to vacuum. We employ this approach to investigate the proton exchange at the anatase-water interface, which is a key process in the acid-base equilibrium of TiO_2 surfaces. The ubiquity of titania in solid-liquid applications has incited the emergence of empirical models to assess the protonation and the dissociation of terminal groups on the TiO_2 surface in aqueous environments.^{20,21} These simple models have been broadly used among experimentalists for the interpretation of their data, but a molecular level description that accounts for the effect of structure has not been established. In this context, the present simulations intend to provide a first-principles glance of the microscopic mechanisms governing the chemistry of this interface.

II. MODEL AND METHODOLOGICAL DISCUSSION

A. About the present implementation and the computational parameters

This model has been implemented in the public domain Car-Parrinello parallel code included in the Quantum-ESPRESSO package,²² based on density-functional theory (DFT), periodic-boundary conditions, plane-waves basis sets, and pseudopotentials to represent the ion-electron interactions. All calculations reported in this work, unless otherwise noted, have been performed using the PW91 exchange-correlation functional²³ in combination with Vanderbilt ultrasoft pseudopotentials.²⁴ The Kohn-Sham orbitals and charge density were expanded in plane waves up to a kinetic energy cutoff of 25 and 200 Ry respectively. Periodic slabs of four layers width representing the (101) surface of the anatase structure were computed using gamma-point sampling in supercells of size 10.24 Å x 7.56 Å x 17.82 Å. For finite temperature (not damped) Car-Parrinello molecular dynamics simulations, an electronic mass of 400 a.u. and a time step of 0.17 fs were adopted. During geometry relaxations and dynamics, all atoms were allowed to move, with the exception of those belonging to the two inner layers, which were fixed in their bulk positions.

B. The continuum solvation model

Within the continuum approach, the solvent is represented as a dielectric medium surrounding a quantum-mechanical solute confined in a cavity. In particular, we consider the polarizable continuum model, in which the dielectric medium and the electronic density respond to the field of each other in a self-consistent fashion. This interaction provides the electrostatic part of the solvation free energy, ΔG_{el} , which is the dominant contribution for polar and charged solutes. The cavitation energy ΔG_{cav} is defined as the work in-

volved in creating the appropriate cavity inside the solution in the absence of solute-solvent interactions.⁷ Electrostatic, cavitation, and dispersion-repulsion effects are modeled as separate contributions,⁷ and the free energy of solvation is regarded as the sum of these three terms ($\Delta G_{sol} = \Delta G_{el} + \Delta G_{cav} + \Delta G_{dis-rep}$). Thermal and pressure dependent terms can also be included but are usually negligible. We note that this decomposition is inherent to the model, being ΔG_{sol} the only measurable quantity.

C. Previous implementation

The starting point for this work is the implementation reported in reference ¹³: in the following paragraphs we revisit those aspects of the preceding version that are essential to the present development. First, we note ΔG_{el} and ΔG_{cav} are considered explicitly, while $\Delta G_{dis-rep}$, less relevant for solutes of moderate size, is largely seized as part of the electrostatic term by virtue of the parametrization. The electrostatic interaction between the dielectric and the solute is calculated as proposed by Fattbert and Gygi,^{11,15} who define the permittivity ϵ of the solvent as a function of the electronic density ρ . Within a pseudopotential framework and in periodic boundary conditions, the Kohn-Sham energy functional²⁵ can be written as

$$E[\rho] = T[\rho] + E_{xc}[\rho] + \frac{1}{2} \int \phi(\mathbf{r})\rho_{tot}(\mathbf{r})d\mathbf{r} + \sum_{I < J} \frac{Z_I Z_J}{R_{IJ}} \operatorname{erfc}\left(\frac{R_{IJ}}{\sqrt{(R_I^c)^2 + (R_J^c)^2}}\right) - \frac{1}{\sqrt{2\pi}} \sum_I \frac{Z_I^2}{R_I^c} + E_{ps}[\rho] \quad (1)$$

where $T[\rho]$ corresponds to the kinetic energy of the electrons and $E_{xc}[\rho]$ to the exchange-correlation energy. The last four terms on the right hand side account for the total electrostatic energy in a periodic crystal, gathering all Coulombic interactions involving electrons and nuclei, only omitting for simplicity the non-local part of the pseudopotential (for a

detailed derivation see reference²⁶ or the Appendix of reference¹³). The electrostatic formulation in Eq. (1) arises from the Ewald sum of point charges, which requires to introduce the ionic densities $\rho_I(\mathbf{r} - \mathbf{R}_I)$ consisting of Gaussian distributions of negative sign that integrate to Z_I , the total charge of the pseudo-ion: $\rho_I(\mathbf{r} - \mathbf{R}_I) = -\frac{Z_I}{(R_I^c)^3} \pi^{-\frac{3}{2}} \exp\left(-\frac{|r-R_I|^2}{(R_I^c)^2}\right)$, with R_I^c the width of the Gaussian associated with the site I .

The third term on the right is conventionally called the Hartree energy:

$$E_H = \frac{1}{2} \int \phi(\mathbf{r}) \rho_{tot}(\mathbf{r}) d\mathbf{r}$$

where ρ_{tot} is just the sum of the electronic plus the ionic densities, $\rho_{tot}(\mathbf{r}) = \rho(\mathbf{r}) + \sum_I \rho_I(\mathbf{r} - \mathbf{R}_I)$, while the electrostatic potential $\phi[\rho]$ is the solution to the Poisson equation in vacuum,

$$\nabla^2 \phi(\mathbf{r}) = -4\pi \rho_{tot}(\mathbf{r}) . \quad (2)$$

In the presence of a dielectric continuum with a permittivity $\epsilon[\rho]$, the Poisson equation becomes

$$\nabla \cdot (\epsilon[\rho] \nabla \phi(\mathbf{r})) = -4\pi \rho_{tot}(\mathbf{r}) . \quad (3)$$

Using Eq. (3), the formula for the Hartree energy E_H , can be integrated by parts to yield:

$$E_H = \frac{1}{8\pi} \int \epsilon[\rho] (\nabla \phi(\mathbf{r}))^2 d\mathbf{r}. \quad (4)$$

The functional derivative of E_H with respect to the charge density is added to the other contributions of the energy (the exchange-correlation, the local and non-local parts of the pseudopotentials) to set up the Kohn-Sham potential $V^{KS}[\rho]$.

$$\frac{\delta E_H}{\delta \rho}(\mathbf{r}) = \phi(\mathbf{r}) + V_\epsilon(\mathbf{r}), \quad (5)$$

$$V_\epsilon(\mathbf{r}) = -\frac{1}{8\pi} (\nabla \phi(\mathbf{r}))^2 \frac{\delta \epsilon}{\delta \rho}(\mathbf{r}). \quad (6)$$

We provide the derivation of Eq. (5) and (6) in the Appendix A, since it is not given in any of the previous references. The dielectric medium and the electronic density respond self-consistently to each other through the dependence of ϵ on ρ and vice versa.

In quantum chemistry continuum models as PCM,^{9,27} the dielectric constant ϵ is taken to be 1 inside the cavity, and a fixed value outside. For molecular dynamics applications, such a discontinuity needs to be removed to calculate accurately the analytic derivatives of the potential with respect to the ionic positions. Besides, in the particular case of plane-waves implementations based on real space grids, a smoothly varying dielectric function is more appropriate for numerical reasons. Fattebert and Gygi proposed the following smoothed step function for the dielectric:

$$\epsilon(\rho(\mathbf{r})) = 1 + \frac{\epsilon_\infty - 1}{2} \left(1 + \frac{1 - (\rho(\mathbf{r})/\rho_0)^{2\beta}}{1 + (\rho(\mathbf{r})/\rho_0)^{2\beta}} \right). \quad (7)$$

This function asymptotically approaches ϵ_∞ (the permittivity of the bulk solvent) in regions of space where the electron density is low, and 1 in those regions where it is high (outside the solvation cavity). The parameter ρ_0 is the density threshold determining the cavity size, whereas β modulates the smoothness of the transition from ϵ_∞ to 1.

On the other hand, the cavitation energy is computed separately as the product between the surface tension of the solvent and the area of the cavity. In this implementation this term remains unchanged; details about the calculation of ΔG_{cav} can be found in reference ¹³.

D. Calculation of periodic slabs: the problem in the convergence

When the scheme described above is applied on structures extended in two dimensions, it typically fails to achieve self-consistency. We found the electrons heat up during the Car-Parrinello relaxation of the wavefunction, causing the total energy to diverge, as shown

in Fig. 1. In other cases the kinetic energy of the electrons is observed to decrease at the beginning, but thereafter experiences irregular oscillations without ever reaching zero. Even if convergence is enforced through the use of a stringent algorithmic strategy, the solution obtained is not reliable, e.g., it depends on the starting conditions or the damping parameters.

The source of this erratic behavior can be tracked to the inclusion of the term V_ϵ in the Kohn-Sham potential. This term, defined in Eq. (6), arises from the dependence of the permittivity on the electron density. Fig. 1 illustrates the impact of this contribution on the convergence of a Car-Parrinello electronic relaxation, by showing that an acceptable dynamics is recovered if V_ϵ is neglected.²⁸ In particular, these results correspond to the anatase-water structure described in section III, but the convergence of other systems is degraded in a similar way. The reason for the instability associated with V_ϵ can be somehow appreciated in the two dimensional plot of Fig. 2, which displays the variation of V_ϵ in the z -direction (the one perpendicular to the surface) at fixed x and y . These coordinates have been chosen to coincide with the position of a Ti atom of the surface. The same graph shows the total Kohn-Sham potential, excluding V_ϵ , so that the relative contribution of this term can be clearly seen. The values are exceptionally large at the solid-liquid boundary, even larger than any of the other contributions to the effective potential. Referenced on the right axis, the dielectric function $\epsilon[\rho]$ is also shown. Since V_ϵ depends on $\partial\epsilon/\partial\rho$ (Eq. 6), the peaks occur at the region where the charge density decays abruptly, producing a rapid variation in $\epsilon[\rho]$ from the value in the solid to the value in the solvent. Adopting the model function of Eq. (7) we have

$$\frac{\partial\epsilon}{\partial\rho}(\mathbf{r}) = \frac{1 - \epsilon_\infty}{\rho_0} \frac{2\beta(\rho(\mathbf{r})/\rho_0)^{2\beta-1}}{(1 + (\rho(\mathbf{r})/\rho_0)^{2\beta})^2}. \quad (8)$$

This expression goes to zero when $\rho(\mathbf{r}) \gg \rho_0$ or $\rho(\mathbf{r}) \ll \rho_0$, and is dominated by $1/\rho_0$

otherwise.²⁹ Then, the extreme values of V_ϵ at the solid-liquid interface ultimately originate in the magnitude of the density threshold ρ_0 . Unfortunately, this parameter may not be freely tuned, but is set in combination with β to fit the experimental data, and no reasonable choice of (ρ_0, β) can be made as to prevent the blowup of V_ϵ . Alternative model functions to represent the dielectric were considered, e.g., with $\epsilon[\rho]$ exhibiting a Gaussian or trigonometric decay with ρ . None of these functions entailed any significant improvement, as far as all of them have in common a sudden change associated with the transition from 1 to ϵ_∞ , which redounds in large values of $\partial\epsilon/\partial\rho$ at the interface. The transition can be smoothed enough as to avoid the sharp peaks in V_ϵ , but in doing so the solvation effect is ruined. Clearly, the discussed behavior is a consequence of the dependence of ϵ on ρ , irrespective of the kind of function chosen to model the dielectric. It should be noticed that the inclusion of V_ϵ does not appear to disturb the convergence or the energy conservation in the case of finite systems, neither in the case of polymers (extended in one dimension).¹⁶ It is seemingly because of the bi-dimensional symmetry of periodic surfaces that V_ϵ turns out to spoil the Car-Parrinello dynamics, by propagating the observed perturbation of the Kohn-Sham potential throughout a full, extended plane.

E. A position dependent formulation

It is fair to wonder about the physical meaning of this strong perturbation of the potential contained in V_ϵ . In the absence of a dielectric, or for a dielectric defined independently of the charge density, the functional derivative of E_H with respect to ρ turns out to be equal to the electrostatic potential $\phi[\rho]$ (see reference³⁰). The additional term V_ϵ emerges from the dependence of E_H on ϵ , whenever ϵ is modeled as a function of the charge density. Since $\partial\epsilon/\partial\rho < 0$ (in Eq. (8), $\epsilon_\infty > 1$), V_ϵ is of a repulsive character. The choice of ρ to delimitate

the region filled by the continuum induces a response of the potential to counteract the strong discontinuity imposed by the same ρ . V_ϵ is such a response, which, throughout the self-consistent procedure, opposes the perturbative drift enforced by the model.

Thus, the instability of the model emanates from the use of the self-consistent charge density to define the dielectric. A possible alternative would be to use instead a non-self consistent, or “fake” density, since the role of the charge density in this context is simply to shape the dielectric medium. As will be discussed below, such an option can be equivalent to define ϵ as a function of the atomic coordinates, which is the usual strategy in quantum chemistry methods. The idea of a dielectric determined by the atomic positions may be less attractive from a physical viewpoint: the size and shape of the cavity depend on the identity of the atoms only, and is not modulated by the electronic structure or the environment; the polarization of the solvent is lost, and, on top of these, many more parameters are needed—at least one per atom. In practice, however, it is possible to choose a dielectric function based on the molecular coordinates that closely reproduces the ρ -dependent solvation, because the effect of the self-consistency and the polarization of the solvent on ΔG_{sol} is quite minor.

In this way, we keep the expression for ϵ given in Eq. (7), but feed it with a dummy density $\gamma(\mathbf{r})$ determined by the ionic positions \mathbf{R}_I ,

$$\gamma(\mathbf{r}) = \sum_I e^{-(|\mathbf{r}-\mathbf{R}_I|-R_{vdw}^I)}, \quad (9)$$

where R_{vdw}^I is the van der Waals radius for the corresponding species. Hence the dielectric function takes the following form:

$$\epsilon(\gamma(\mathbf{r})) = 1 + \frac{\epsilon_\infty - 1}{2} \left(1 + \frac{1 - \gamma(\mathbf{r})^{2\beta}}{1 + \gamma(\mathbf{r})^{2\beta}} \right). \quad (10)$$

Using this definition, the transition of $\epsilon(\gamma(\mathbf{r}))$ between 1 and ϵ_∞ is centered around the van der Waals radius. Aside from R_{vdw}^I , which values are tabulated, β is left as the only

adjustable parameter to fit the experimental solvation energies. Fig. 3 shows the aspect of the dielectric function around an oxygen atom for different β . This parameter must be large enough to ensure most of the transition occurs within a small length window, but at the same time the numerical accuracy needs to be preserved, so there is an upper bound for β which depends on the given grid size.

Within this framework, the electrostatic contribution to $V^{KS}[\rho]$ is simply the electrostatic potential $\phi[\rho]$, and the stability of Car-Parrinello dynamics in periodic slabs is recovered. Table I presents, for several neutral and charged solutes, a comparison between the values of ΔG_{sol} obtained with the dielectric functions of Eq. (7) and Eq. (10), respectively. The small differences proceed exclusively from ΔG_{el} , since ΔG_{cav} is the same in both cases ($\Delta G_{sol} = \Delta G_{el} + \Delta G_{cav}$). As mentioned above, with a proper choice of β the position dependent dielectric is able to provide solvation energies in close agreement with the previous model and with experiments. The results shown correspond to $\beta = 2.4$.

The explicit dependence of ϵ on the ionic positions involves a new contribution to the forces arising from the derivative of E_H with respect to \mathbf{R}_I , which must be taken into account to perform conservative molecular dynamics simulations. After some manipulation involving the use of Eqs. (3) and (4), this derivative can be expressed as follows (the full derivation is given in Appendix B):

$$\frac{\partial E_H}{\partial \mathbf{R}_I} = -\frac{1}{8\pi} \int \frac{\partial \epsilon(\mathbf{R}_I)}{\partial \mathbf{R}_I} (\nabla \phi(\mathbf{r}))^2 d\mathbf{r} + \int \phi(\mathbf{r}) \frac{\partial \rho_{tot}(\mathbf{r})}{\partial \mathbf{R}_I} d\mathbf{r} \quad (11)$$

The computation of the first term on the right is straightforward since we know, from Eqs. (9) and (10), the explicit dependence of ϵ on \mathbf{R}_I :

$$\frac{\partial \epsilon(\mathbf{R}_I)}{\partial \tau_I}(\mathbf{r}) = 2\beta (\epsilon_\infty - 1) \left(\frac{\tau - \tau_0}{R} \right) \frac{e^{-(R-R_{vdw}^I)} \left(\sum_I e^{-(R-R_{vdw}^I)} \right)^{2\beta-1}}{\left[1 + \left(\sum_I e^{-(R-R_{vdw}^I)} \right)^{2\beta} \right]^2} \quad (12)$$

with τ a generic coordinate x, y , or z , $\mathbf{R}_I = (x_0, y_0, z_0)$ and $R = |\mathbf{r} - \mathbf{R}_I|$.

On the other hand, if $\phi(\mathbf{r})$ is transformed to Fourier space so that $\phi(\mathbf{r}) = \sum_{\mathbf{G}} \tilde{\phi}(\mathbf{G})e^{i\mathbf{G}\mathbf{r}}$ (see next section), the second term in Eq. (11) can be evaluated as

$$\int \phi(\mathbf{r}) \frac{\partial \rho_{tot}(\mathbf{r})}{\partial \mathbf{R}_I} d\mathbf{r} = -\Omega \sum_{\mathbf{G}} i\mathbf{G} \tilde{\phi}^*(\mathbf{G}) \tilde{\rho}_I(\mathbf{G}) e^{-i\mathbf{G}\mathbf{R}_I} \quad (13)$$

with $\tilde{\rho}_I(\mathbf{G})$ the form factor of the ionic densities, $\rho_I(\mathbf{r} - \mathbf{R}_I) = \sum_{\mathbf{G}} \tilde{\rho}_I(\mathbf{G}) e^{-i\mathbf{G}\mathbf{r}} e^{-i\mathbf{G}\mathbf{R}_I}$.

To ensure the conservation of the total energy during the molecular dynamics simulations, the contributions given in Eqs. (12) and (13) must take the place of the derivative of the Hartree energy in the absence of the dielectric:

$$\frac{\partial E_H}{\partial \mathbf{R}_I} = -4\pi\Omega \sum_{\mathbf{G}} i\mathbf{G} \left(\frac{\tilde{\rho}^*(\mathbf{G})}{G^2} \right) \tilde{\rho}_I(\mathbf{G}) e^{-i\mathbf{G}\mathbf{R}_I}. \quad (14)$$

F. The multigrid scheme and a mixed strategy to solve the Poisson problem

In standard plane waves codes based on real space grids, the electrostatic potential $\phi(\mathbf{r})$ is obtained from the Poisson equation (2), which can be efficiently inverted with the use of fast Fourier transforms (FFT). Both the total charge density $\rho_{tot}(\mathbf{r})$ and $\phi(\mathbf{r})$ can be expanded in plane waves,

$$\rho_{tot}(\mathbf{r}) = \sum_{\mathbf{G}} \tilde{\rho}(\mathbf{G}) e^{i\mathbf{G}\mathbf{r}}, \quad \phi(\mathbf{r}) = \sum_{\mathbf{G}} \tilde{\phi}(\mathbf{G}) e^{i\mathbf{G}\mathbf{r}}.$$

Replacing into the Poisson equation $\nabla^2 \phi = -4\pi \rho_{tot}$, and equating coefficients:

$$\mathbf{G}^2 \tilde{\phi}(\mathbf{G}) = 4\pi \tilde{\rho}(\mathbf{G}) \quad , \quad \phi(\mathbf{r}) = \sum_{\mathbf{G}} \frac{4\pi}{\mathbf{G}^2} \tilde{\rho}(\mathbf{G}) e^{i\mathbf{G}\mathbf{r}} \quad (15)$$

Unfortunately, the Poisson equation in the presence of an arbitrary dielectric, Eq. (3), can not be addressed in the same way, and an alternative numerical scheme is required. To that end, we have implemented from scratch a sixth-order multigrid code,³¹ which solves in real space the Poisson equation with non-constant coefficients and periodic boundary conditions.

Eq. (3) can be rewritten as:

$$\frac{\partial \epsilon}{\partial x} \frac{\partial \phi}{\partial x} + \frac{\partial \epsilon}{\partial y} \frac{\partial \phi}{\partial y} + \frac{\partial \epsilon}{\partial z} \frac{\partial \phi}{\partial z} + \epsilon \left(\frac{\partial^2 \epsilon}{\partial x^2} + \frac{\partial^2 \epsilon}{\partial y^2} + \frac{\partial^2 \epsilon}{\partial z^2} \right) = -4\pi\rho. \quad (16)$$

This equation is developed in finite differences, expanding the derivatives of ϕ and ϵ to sixth-order according to the following relations for the gradient and the Laplacian:

$$\frac{\partial f(\mathbf{r})}{\partial \tau} = \frac{1}{h} \sum_{n=-3}^3 \alpha_n u_{i+n} + O(h^7) \quad (17)$$

$$\frac{\partial^2 f(\mathbf{r})}{\partial \tau^2} = \frac{1}{h^2} \sum_{n=-3}^3 \beta_n u_{i+n} + O(h^7) \quad (18)$$

where τ is a generic coordinate x, y , or z ; h is the grid spacing in the direction τ ; and u is the discretization of a continuous function $f(\mathbf{r})$, representing $\phi(\mathbf{r})$, $\rho(\mathbf{r})$, or $\epsilon(\mathbf{r})$. u_i refers to u evaluated at a mesh point associated with \mathbf{r} , while u_{i+n} corresponds to a neighboring point n positions to the right in the direction τ (if $n < 0$, u_{i+n} is located to the left of u_i).

The coefficients α_n and β_n are given by:

$$\alpha_0 = 0, \quad \alpha_1 = \frac{3}{4}, \quad \alpha_2 = -\frac{3}{20}, \quad \alpha_3 = \frac{1}{60}, \quad \alpha_{-n} = -\alpha_n$$

$$\beta_0 = -\frac{49}{18}, \quad \beta_1 = \frac{27}{18}, \quad \beta_2 = -\frac{27}{180}, \quad \beta_3 = \frac{2}{180}, \quad \beta_{-n} = \beta_n.$$

In the case of $\epsilon(\mathbf{r}) = 1$ for all \mathbf{r} , this method provides a solution for $\phi(\mathbf{r})$ which is indistinguishable from the one obtained with FFT. It also demonstrated an excellent performance when tried on functions with non-constant coefficients and oscillation frequencies comparable to those of interest. For example, for $\phi = e^{-ar}$ and $\epsilon = e^{-br}$ ($0.5 < a, b < 2.0$) the relative error in $\phi(\mathbf{r})$ was less than 10^{-4} in a mesh of $80 \times 80 \times 80$ points.

At the initial steps of a molecular dynamics simulation, the convergence of the potential may require 15-30 multigrid cycles. Given the self-consistent nature of the procedure, however, after a few time steps the number of cycles necessary to reach convergence is typically

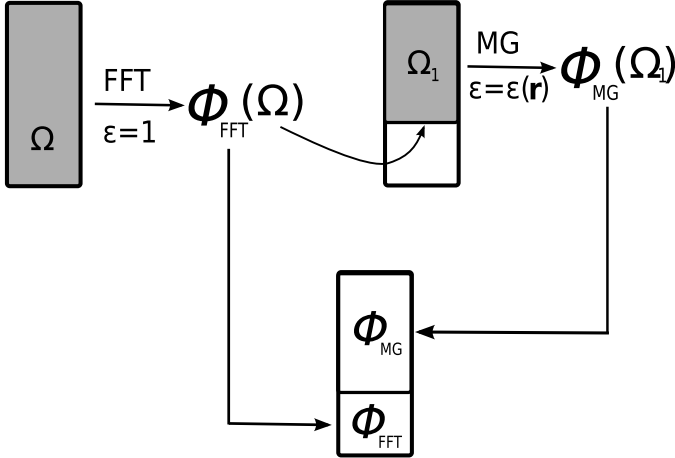
decreased to less than five. Even so, the multigrid algorithm is still significantly more expensive than FFTs. Propitiously, multigrid methods can be adapted to any kind of boundary conditions, and this feature can be exploited to reduce the size of the mesh involved. To implement this idea, a region in the supercell—preferably the slab—must remain inaccessible to the solvent, so that $\epsilon(\mathbf{r}) = 1$ within it. In practice, the dielectric function of Eqs. (7) or (10) is not diffuse enough as to encompass all the volume of the slab—if it were, the solvation effect would fade at the molecular boundaries—, so the solvent occupies the interstitial space left by the atomic structure (Fig. 4a). This is inconvenient not only because it increases the numerical complexity of the problem, but also because it is not physical, i.e., the solvent does not penetrate the atomic structure of the surface. A simple device to exclude the solvent from the solid interspaces is to modify $\gamma(\mathbf{r})$ in the following way:

$$\gamma(\mathbf{r}) = \begin{cases} \sum_I e^{-\left(|\mathbf{r}-\mathbf{R}_I|-R_{vdw}^I\right)} & z_I > z_{lim} \\ \sum_I e^{-\frac{z-z_I}{|z-z_I|}\left(|\mathbf{r}-\mathbf{R}_I|-R_{vdw}^I\right)} & z_I \leq z_{lim} \end{cases} \quad (19)$$

where z_I is the z -component of \mathbf{R}_I (we recall z is the coordinate perpendicular to the surface; it is zero at the bottom of the unit cell and maximum at the top). The factor $\frac{z-z_I}{|z-z_I|}$ produces a rapid increase in $\gamma(\mathbf{r})$ underneath the atom I , which saturates the value of $\epsilon(\mathbf{r})$ for all atoms I located below z_{lim} . Thus, only the upper face of the slab is in contact with the solution, the dielectric function becoming equal to 1 throughout the lower section of the supercell. Fig. 4b depicts $\epsilon(\mathbf{r})$ when z_{lim} is chosen equal to the z coordinate of an ion belonging to the second layer.

Under these conditions, it is possible to solve the Poisson problem in two steps: first, the potential $\phi(\mathbf{r})$ is computed for $\epsilon = 1$ in the full domain Ω using FFTs; secondly, $\phi(\mathbf{r})$ is recalculated in the presence of the dielectric with the multigrid method but in a smaller domain Ω_1 , imposing the boundary conditions proceeding from the FFT solution. The sub-

domain Ω_1 must be chosen in such a way that it overlaps with a sub-space where $\epsilon(\mathbf{r}) = 1$, so that the boundary conditions for the multigrid are given by the solution of the Poisson equation in vacuum. Then, the total potential is constructed from the combination of the multigrid solution in Ω_1 plus the FFT solution in the rest of the space. The full procedure is summarized in Scheme 1.

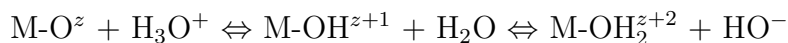


Scheme 1

In proposing this approach, we assume the dielectric effect is mostly local and does not perturb the electrostatic potential deep inside the slab. More formally, this implies that even in the presence of the dielectric medium, there is a region in the real space grid where the self-consistent potential is exactly the same as the potential corresponding to vacuum. It is therefore important that Ω_1 extends sufficiently down into the surface as to reach that region. With this mixed scheme, the size of the mesh to be submitted to the multigrid routine can be reduced up to 40 %.

III. APPLICATIONS: MOLECULAR DYNAMICS AT THE TiO_2 INTERFACE

It is well known that surface groups of most inorganic oxides ionize in solution, exhibiting the following equilibria:



with z the surface group charge, which can be negative, positive, or zero, depending on the nature of the oxide.²¹ Understanding the acid-base behavior resulting from these equilibria is crucial in almost every application of these materials in solution. Isoelectric points of many oxides have been known for years,³² however, it is very difficult to probe the surface of bulk materials or nanoparticles in solution, and most of the data collected corresponds to the average behavior of the different surfaces exposed in a given experiment. More recently, researchers have sought to take advantage of density functional theory to establish the degree of dissociation and protonation at different titania-water interfaces with an explicit representation of the solvent.^{33–35} For the reasons already discussed, such an approach is costly and has been employed only in a limited number of cases. In what follows, we apply our continuum solvent model to characterize the hydrated (101) surface of the anatase structure of TiO_2 , which is possibly the most stable and abundant.⁴ The adsorption of H_2O on perfect TiO_2 surfaces in the gas phase has been thoroughly investigated using both experimental and theoretical approaches.^{36–41} In the case of the (101) face of anatase, there is consensus in the fact that molecular adsorption of water is thermodynamically the most stable. Electronic structure calculations suggest that the difference between the two possible adsorption modes—molecular versus dissociated—is of nearly 10 kcal/mol.³⁹ We have performed calculations in four layers slabs representing the (101) surface of the anatase structure. As previously reported, our own calculations in vacuum summarized in Table II show that at different water coverages, the molecular pathway is the most favored. The same trend prevails in the presence of the solvent, although the interaction energies with the surface turn out to be significantly lower. Table II presents the results from geometry optimizations of the fully hydrated surface embedded in the continuum dielectric. The

observed weakening of the interaction with the oxide with respect to vacuum is a consequence of the stabilization of the H_2O molecules in the polar environment, and can be understood in terms of a competition between the bulk solvent and the surface for the water molecules. Despite this lower affinity, the massive presence of water from the liquid phase will displace the equilibrium toward the formation of an adsorbed monolayer. The energy difference between the two kinds of mechanisms remains about the same as in the gas phase, the dissociative adsorption becoming exothermic. In solution, however, dissociation is likely to occur, controlled by the pH of the medium (see below).

The quantitative effect of pH on the ionization of the surface is quite difficult to assess from first principles simulations, since a huge supercell would be needed to have a meaningful representation of the proton concentration in the system. In this preliminary study, we limit ourselves to examine the proton exchange between an adsorbed water molecule and an hydroxyl anion from the solution, using molecular dynamics at 300 K. This computational experiment is meant to provide a qualitative picture of the abstraction of a proton from the surface in the presence of OH^- , illustrating at the same time the performance of the continuum solvent method. The inset of Fig. 5 shows the evolution of the dynamics through a sequence of photos, starting at an initial configuration in which an OH^- group exhibits an H-bond with an adsorbed water molecule. Early in the simulation, the covalent O-H bond in H_2O is disrupted, to leave an hydroxyl function on the surface and a newly formed water molecule that soon wanders around the liquid phase. Fig. 5 presents the $\text{O}_a\text{-H}_a$ and $\text{O}_b\text{-H}_a$ distances, where O_a and O_b are the oxygen atoms of the (initially) adsorbed water molecule and the hydroxide, respectively, and H_a is the abstracted proton. For this reaction to occur in a reasonable time as to be within reach of molecular dynamics simulations, the starting geometry must be chosen appropriately. As a matter of fact, had the simulation

been started from a random configuration, the OH^- anion might have explored the supercell for several picoseconds without ever reacting with the water molecule. In the absence of the solvent, instead, the unscreened interaction between the hydroxide and the surface leads to an immediate reaction. This distinctive behavior is displayed in Fig. 6, which presents the $\text{O}_b\text{-H}_a$ distances for two simulations, one in vacuum and the other in solution, started from the same geometry and with identical computational parameters. The observed contrast between the two dynamics evinces how the dielectric medium stabilizes the hydroxide in the liquid phase. The use of this kind of methodology in combination with weighted importance sampling techniques (e.g., Umbrella sampling)⁴² could provide estimates for the acid-base equilibrium constants corresponding to different oxide surfaces and phases. We believe this direction, even though beyond the scope of the present work—with an emphasis on the methodological conception—aims to a very appealing ground for future research.

IV. CLOSING REMARKS

We have shown that a dielectric medium defined as a function of the self-consistent charge density provokes a strong response in the effective potential, which in solid-liquid systems may spoil the convergence of the Car-Parrinello electronic dynamics. Such a response can be avoided with a dielectric based on a non self-consistent charge, preserving in this way the potential and allowing for conservative molecular dynamics simulations. This approach is equivalent to have a position-dependent permittivity, and therefore a new term in the ionic forces must be considered.

The methodology presented here is a powerful instrument to explore the thermodynamics and the reactivity of surfaces and nanoparticles in solution. Replacement of the solvent molecules by a dielectric continuum may neglect the structural features of the liquid phase,

but it does capture the essential polarization effect of the medium. This is manifest, for instance, in the charge of the hydroxyl group: if an additional electron is added to a neutral system consisting of a slab plus a (distant) OH moiety in vacuum, a significant portion of the charge flows to the solid phase. Noticeably, in the presence of the solvent, the excess electron spontaneously localizes on the hydroxyl. This is quantitatively depicted in Fig. 7.

A compelling application for this continuum solvent scheme, as well as a natural continuation of this work, would be the characterization of the adsorption energies and geometries of water and other species on the different surfaces of titanium dioxide. We deem especially worthwhile the calculation of the reaction energies for the kind of equilibria mentioned above, e.g., $\text{Ti-OH}_2 + \text{OH}^- \Leftrightarrow \text{Ti-OH}^- + \text{H}_2\text{O}$, as a function of the surface structure. Work in this direction is now in progress. At this point it should be noted that it would be not feasible to have an estimate of these quantities without the solvation model: in the absence of the dielectric, the interaction between the surface and the OH^- ion (or between the charged slab and the water molecule) is extremely dependent on the distance separating them, and therefore it is not possible to establish unequivocally the energies for reactants and products. When the dielectric is included, the long range interaction between charged and polar fragments is efficiently screened, and the total energy of the system becomes independent of the position of the molecule (or the ion) with respect to the slab. This property makes possible to evaluate reaction energies on periodic surfaces in solution which could not be calculated by other means, except perhaps with extensive molecular dynamics simulations. Aside from these, the scheme presented here would be particularly useful to assess the role of the solvent in a great diversity of problems in surface chemistry, including the effects on structure, on vibrational frequencies, or on charge transfer phenomena, among many others.

V. ACKNOWLEDGMENTS

We feel indebted to Jean-Luc Fattebert, Oswaldo Dieguez, Ismailia Dabo, Nicola Marzari, and Patu Groisman, for precious advice and enlightening discussions. This study has been financially supported by CONICET (PIP-5220) and by the Agencia Nacional de Promoción Científica y Tecnológica (PICT 06-33581). V.M.S. acknowledges CONICET for a doctoral fellowship.

VI. APPENDIX A: FUNCTIONAL DERIVATIVE OF V_ϵ

Following Parr and Yang,³⁰ the functional derivative of $E_H[\rho]$ with respect to $\rho(\mathbf{r})$, which we will denote $\frac{\delta E_H}{\delta \rho}$, is defined by the relation

$$\lim_{\lambda \rightarrow 0} \left[\frac{E_H(\rho + \lambda f) - E_H(\rho)}{\lambda} \right] = \int \frac{\delta E_H}{\delta \rho} f(\mathbf{r}) d\mathbf{r} \quad (20)$$

where $f(\mathbf{r})$ is arbitrary. From the definition of $E_H[\rho]$ we can write

$$\begin{aligned} 2E_H(\rho + \lambda f) - 2E_H(\rho) &= \int \phi_{\rho+\lambda f}(\rho + \lambda f) d\mathbf{r} - \int \phi_\rho \rho d\mathbf{r} \\ &= \int \phi_{\rho+\lambda f} \rho d\mathbf{r} + \lambda \int \phi_{\rho+\lambda f} f d\mathbf{r} - \int \phi_\rho \rho d\mathbf{r} = \lambda \int \phi_{\rho+\lambda f} f d\mathbf{r} + \int (\phi_{\rho+\lambda f} - \phi_\rho) \rho d\mathbf{r}. \end{aligned} \quad (21)$$

In the last term above ρ can be rewritten using Eq. (3), and the resulting expression can be integrated by parts (from now on we omit $d\mathbf{r}$ from the integrand for conciseness):

$$\begin{aligned} \int (\phi_{\rho+\lambda f} - \phi_\rho) \rho &= -\frac{1}{4\pi} \int (\phi_{\rho+\lambda f} - \phi_\rho) \nabla (\epsilon_\rho \nabla \phi_\rho) \\ &= \frac{1}{4\pi} \int \nabla \phi_{\rho+\lambda f} \epsilon_\rho \nabla \phi_\rho - \frac{1}{4\pi} \int \nabla \phi_\rho \epsilon_\rho \nabla \phi_\rho \\ &= \frac{1}{4\pi} \int \nabla \phi_{\rho+\lambda f} (\epsilon_\rho - \epsilon_{\rho+\lambda f}) \nabla \phi_\rho + \frac{1}{4\pi} \int \nabla \phi_{\rho+\lambda f} \epsilon_{\rho+\lambda f} \nabla \phi_\rho - \frac{1}{4\pi} \int \nabla \phi_\rho \epsilon_\rho \nabla \phi_\rho \\ &= \frac{1}{4\pi} \int \nabla \phi_{\rho+\lambda f} (\epsilon_\rho - \epsilon_{\rho+\lambda f}) \nabla \phi_\rho + \int (\rho + \lambda f) \phi_\rho - \frac{1}{4\pi} \int \epsilon_\rho (\nabla \phi_\rho)^2. \end{aligned}$$

To arrive to the last expression, $\epsilon_{\rho+\lambda f}$ was added and subtracted in the third equality, and then the second term was integrated by parts. This result can now be inserted in Eq. (21):

$$2E_H(\rho + \lambda f) - 2E_H(\rho) = \lambda \int \phi_{\rho+\lambda f} f + \frac{1}{4\pi} \int \nabla \phi_{\rho+\lambda f} (\epsilon_\rho - \epsilon_{\rho+\lambda f}) \nabla \phi_\rho + \lambda \int f \phi_\rho + \int \rho \phi_\rho - \frac{1}{4\pi} \int \epsilon_\rho (\nabla \phi_\rho)^2 = \lambda \int (\phi_{\rho+\lambda f} + \phi_\rho) f - \frac{1}{4\pi} \int \nabla \phi_{\rho+\lambda f} (\epsilon_{\rho+\lambda f} - \epsilon_\rho) \nabla \phi_\rho \quad (22)$$

Dividing Eq. (22) by 2λ , and taking the limit ($\lambda \rightarrow 0$), we get to the final outcome:

$$\begin{aligned} \lim_{\lambda \rightarrow 0} \left[\frac{E_H(\rho + \lambda f) - E_H(\rho)}{\lambda} \right] &= \lim_{\lambda \rightarrow 0} \left[\frac{1}{2} \int (\phi_{\rho+\lambda f} + \phi_\rho) f - \frac{1}{8\pi} \int \nabla \phi_{\rho+\lambda f} \nabla \phi_\rho \frac{(\epsilon_{\rho+\lambda f} - \epsilon_\rho)}{\lambda} \right] \\ &= \int \phi_\rho f - \frac{1}{8\pi} \int \nabla \phi_\rho \nabla \phi_\rho \frac{\partial \epsilon}{\partial \rho} f = \int (\phi_\rho - \frac{1}{8\pi} (\nabla \phi_\rho)^2 \frac{\partial \epsilon}{\partial \rho}) f(\mathbf{r}) d\mathbf{r}. \end{aligned} \quad (23)$$

By comparison with Eq. (20), it is easy to see that $\frac{\partial E_H}{\partial \rho} = \phi_\rho - \frac{1}{8\pi} (\nabla \phi_\rho)^2 \frac{\partial \epsilon}{\partial \rho}$.

VII. APPENDIX B: DERIVATIVE OF E_H WITH RESPECT TO THE IONIC POSITIONS

In the absence of a dielectric ($\epsilon = 1$), Eq. (15) can be inserted in the expression for the Hartree energy to give

$$E_H = 2\pi\Omega \sum_{\mathbf{G}} \frac{|\tilde{\rho}(\mathbf{G})|^2}{G^2} \quad (24)$$

where $\tilde{\rho}(\mathbf{G})$ are the Fourier coefficients for the expansion of $\rho_{tot}(\mathbf{r})$, $\tilde{\rho}(\mathbf{G}) = \tilde{\rho}_e(\mathbf{G}) + \sum_I \tilde{\rho}_I(\mathbf{G}) e^{-i\mathbf{G}\mathbf{R}_I}$. Since the only explicit dependence of $\tilde{\rho}(\mathbf{G})$ on $\{\mathbf{R}_I\}$ is through the structure factor ($e^{-i\mathbf{G}\mathbf{R}_I}$), the derivative of Eq. (24) with respect to the atomic positions is just

$$\frac{\partial E_H}{\partial \mathbf{R}_I} = -4\pi\Omega \sum_{\mathbf{G}} i\mathbf{G} \left(\frac{\tilde{\rho}^*(\mathbf{G})}{G^2} \right) \tilde{\rho}_I(\mathbf{G}) e^{-i\mathbf{G}\mathbf{R}_I}. \quad (25)$$

In the presence of a dielectric medium determined by the ionic coordinates, Eq. (24) does not hold. To calculate $\partial E_H / \partial \mathbf{R}_I$ we replace $\epsilon[\rho]$ for $\epsilon(\mathbf{R}_I)$ in Eq. (4) and derivate:

$$\frac{\partial E_H}{\partial \mathbf{R}_I} = \frac{1}{8\pi} \int \frac{\partial \epsilon(\mathbf{R}_I)}{\partial \mathbf{R}_I} (\nabla \phi(\mathbf{r}))^2 d\mathbf{r} + \frac{1}{8\pi} \int \epsilon(\mathbf{R}_I) \frac{\partial (\nabla \phi(\mathbf{r}))^2}{\partial \mathbf{R}_I} d\mathbf{r}. \quad (26)$$

The second term on the right member can be further developed as follows:

$$\begin{aligned} \frac{1}{8\pi} \int \epsilon(\mathbf{R}_I) \frac{\partial(\nabla\phi(\mathbf{r}))^2}{\partial\mathbf{R}_I} d\mathbf{r} &= \frac{2}{8\pi} \int \epsilon(\mathbf{R}_I) \nabla\phi(\mathbf{r}) \left(\nabla \frac{\partial\phi(\mathbf{r})}{\partial\mathbf{R}_I} \right) d\mathbf{r} = \\ &- \frac{1}{4\pi} \int \nabla \cdot [\epsilon(\mathbf{R}_I) \nabla\phi(\mathbf{r})] \frac{\partial\phi(\mathbf{r})}{\partial\mathbf{R}_I} d\mathbf{r} = \int \rho_{tot}(\mathbf{r}) \frac{\partial\phi(\mathbf{r})}{\partial\mathbf{R}_I} d\mathbf{r} \end{aligned} \quad (27)$$

where we have integrated by parts and used Eq. (3). Then, it is possible to rewrite (26):

$$\frac{\partial E_H}{\partial\mathbf{R}_I} = \frac{1}{8\pi} \int \frac{\partial\epsilon(\mathbf{R}_I)}{\partial\mathbf{R}_I} (\nabla\phi(\mathbf{r}))^2 d\mathbf{r} + \int \rho_{tot}(\mathbf{r}) \frac{\partial\phi(\mathbf{r})}{\partial\mathbf{R}_I} d\mathbf{r}. \quad (28)$$

On the other hand, the derivation of the general expression for the Hartree energy leads to:

$$\frac{\partial E_H}{\partial\mathbf{R}_I} = \frac{1}{2} \int \rho_{tot}(\mathbf{r}) \frac{\partial\phi(\mathbf{r})}{\partial\mathbf{R}_I} d\mathbf{r} + \frac{1}{2} \int \phi(\mathbf{r}) \frac{\partial\rho_{tot}(\mathbf{r})}{\partial\mathbf{R}_I} d\mathbf{r}. \quad (29)$$

Equating (28) and (29) we find the following relation:

$$\int \rho_{tot}(\mathbf{r}) \frac{\partial\phi(\mathbf{r})}{\partial\mathbf{R}_I} d\mathbf{r} = -\frac{1}{4\pi} \int \frac{\partial\epsilon(\mathbf{R}_I)}{\partial\mathbf{R}_I} (\nabla\phi(\mathbf{r}))^2 d\mathbf{r} + \int \phi(\mathbf{r}) \frac{\partial\rho_{tot}(\mathbf{r})}{\partial\mathbf{R}_I} d\mathbf{r}. \quad (30)$$

Ultimately, replacing (30) into (28) we obtain the final result,

$$\frac{\partial E_H}{\partial\mathbf{R}_I} = -\frac{1}{8\pi} \int \frac{\partial\epsilon(\mathbf{R}_I)}{\partial\mathbf{R}_I} (\nabla\phi(\mathbf{r}))^2 d\mathbf{r} + \int \phi(\mathbf{r}) \frac{\partial\rho_{tot}(\mathbf{r})}{\partial\mathbf{R}_I} d\mathbf{r}. \quad (31)$$

-
- ¹ Science special issue 5890, August 2008. See in particular: E. A. Carter, *Science* **321**, 800 (2008); G. J. Kroes, *Science* **321**, 794 (2008).
- ² L. W. Bruch, R. D. Diehl, and J. A. Venables, *Rev. Mod. Phys.* **79**, 1381 (2007).
- ³ A. Nilsson and L. G. M. Pettersson, *Surf. Sci. Rep.* **55**, 49 (2004).
- ⁴ U. Diebold, *Surf. Sci. Rep.* **48**, 53 (2003).
- ⁵ It is possible to find in the literature a few number of studies in which one or several layers of water molecules are incorporated to represent the solvent. See for example A. Tilocca and A. Selloni, *Langmuir* **20**, 8379 (2004); A. B. Mukhopadhyay, C. B. Musgrave, and J. Fdez. Sanz, *J. Am. Chem. Soc.* **130**, 11996 (2008).
- ⁶ C. J. Cramer and D. G. Truhlar, *Chem. Rev.* **99**, 2161 (1999).
- ⁷ I. N. Levine, *Quantum Chemistry* (Prentice Hall, New Jersey, 2000).
- ⁸ T. Schlick, *Molecular Modeling and Simulation* (Springer-Verlag, New York, 2002).
- ⁹ J. Tomasi, B. Mennucci, and R. Cammi, *Chem. Rev.* **105**, 2999 (2005).
- ¹⁰ F. De Angelis, A. Sgamellotti, M. Cossi, N. Rega, and V. Barone, *Chem. Phys. Lett.* **328**, 302 (2000).
- ¹¹ J.-L. Fattebert and F. Gygi, *Int. J. Quantum Chem.* **93**, 139 (2003).
- ¹² H. Martin Senn, P. M. Margi, R. Schmid, T. Ziegler, and P. Blöchl, *J. Chem. Phys.* **118**, 1089 (2003).
- ¹³ D. A. Scherlis, J.-L. Fattebert, F. Gygi, M. Cococcioni, and N. Marzari, *J. Chem. Phys.* **124**, 74103 (2006).
- ¹⁴ T. Arias and co-workers have devised a form of density functional theory for the self-consistent

- embedding of quantum-mechanical systems in a dielectric medium. This approach has been applied to investigate the atomic and electronic structure of the Cr_2O_3 surface in solution by means of static calculations. See S. A. Petrosyan, A. A. Rigos, and T. A. Arias, *J. Phys. Chem. B* **109**, 15436 (2005); S. A. Petrosyan, J.-F. Briere, D. Roundy, and T. A. Arias, *Phys. Rev. B* **75**, 205105 (2007).
- ¹⁵ J.-L. Fattebert and F. Gygi, *J. Comput. Chem.* **23**, 662 (2002).
- ¹⁶ D. A. Scherlis, J.-L. Fattebert, and N. Marzari, *J. Chem. Phys.* **124**, 194902 (2006).
- ¹⁷ W. H. Press, S. A. Teukolsky, W. T. Vetterling, and B. P. Flannery, *Numerical Recipes in Fortran*, 2nd Ed. (Cambridge University Press, New York, 1992).
- ¹⁸ W. L. Briggs, V. Emden Henson, and S. F. McCormick, *A Multigrid Tutorial*, 2nd Ed. (SIAM, Philadelphia, 2000).
- ¹⁹ U. Trottenberg, C. W. Oosterlee, and A. Schüller, *Multigrid* (Elsevier Academic Press, San Diego, 2001).
- ²⁰ T. Hiemstra, P. Venema, W. H. Van Riemsdijk, *J. Colloid Interface Sci.* **184**, 680 (1996).
- ²¹ J.-P. Jolivet, *Metal Oxide Chemistry and Synthesis* (John Wiley & Sons, Chichester, 2000).
- ²² S. Baroni, A. Dal Corso, S. de Gironcoli, P. Giannozzi, C. Cavazzoni, G. Ballabio, S. Scandolo, G. Chiarotti, P. Focher, A. Pasquarello, K. Laasonen, A. Trave, R. Car, N. Marzari, A. Kokalj, <http://www.quantum-espresso.org/>.
- ²³ J. P. Perdew, in *Electronic Structure of Solids '91*, edited by P. Ziesche and H. Eschrig (Akademie Verlag, Berlin, 1991).
- ²⁴ D. Vanderbilt, *Phys. Rev. B* **41**, 7892 (1990).
- ²⁵ D. Marx and J. Hutter. Ab initio molecular dynamics: Theory and Implementation, in *Modern Methods and Algorithms of Quantum Chemistry* (J. Grotendorst Ed., John Von Neumann

- Institute for Computing, Jülich, 2000).
- ²⁶ G. Galli and A. Pasquarello. First-principles Molecular Dynamics, in *Computer Simulation in Chemical Physics* (M.P. Allen and D.J. Tildesley Eds., Kluwer Academic Publishers, The Netherlands, 1993).
- ²⁷ M. Cossi, V. Barone, R. Cammi, and J. Tomasi, Chem. Phys. Lett. **255**, 327 (1996).
- ²⁸ Of course, the mere omission of V_ϵ would not be an acceptable solution, since the energy conservation will be affected.
- ²⁹ The parameter β is taken greater than 0.5. See reference¹⁵.
- ³⁰ R. G. Parr and W. Yang, *Density-Functional Theory of Atoms and Molecules* (Oxford University Press, New York, 1989).
- ³¹ Multigrid methods solve elliptic partial differential equations by applying a classic finite-differences iterative technique in meshes of different sizes (in this case we adopt the Gauss-Seidel scheme). See reference¹⁷ for an introduction, reference¹⁸ or¹⁹ for more specialized sources.
- ³² G. A. Parks, Chem. Rev. **65**, 177 (1965).
- ³³ A. V. Bandura, D. G. Sykes, V. Shapovalov, T. N. Troung, J. D. Kubicki, and R. A. Evarestov, Langmuir **108**, 7844 (2004).
- ³⁴ A. Tilocca and A. Selloni, J. Phys. Chem. B **108**, 4743 (2004)
- ³⁵ M. L. Machesky, M. Pedota, D. J. Wesolowski, L. Vlcek, P. T. Cummings, J. Rosenqvist, M. K. Ridley, J. D. Kubicki, A. V. Bandura, N. Kumar, and J. O. Sofo, Langmuir **24**, 12331 (2008).
- ³⁶ M. A. Henderson, Surf. Sci. **355**, 151 (1996).
- ³⁷ R. Schaub, P. Thostrup, N. Lopez, E. Laegsgaard, I. Stensgaard, J. K. Nørskov, and F. Besenbacher, Phys. Rev. Lett. **87**, 266104 (2001).
- ³⁸ G. Li, L. Li, J. Boerio-Goates, and B. F. Woodfield, J. Am. Chem. Soc. **127**, 8659 (2005).

- ³⁹ A. Vittadini, A. Selloni, F. P. Rotzinger, and M. Grätzel, *Phys. Rev. Lett.* **81**, 2954 (1998).
- ⁴⁰ A. Tilocca and A. Selloni, *J. Chem. Phys.* **119**, 7445 (2003).
- ⁴¹ P. J. D. Lindan and C. Zhang, *Phys. Rev. B* **72**, 75439 (2005).
- ⁴² G. M. Torrie and J. P. Valleau, *J. Comp. Phys.* **23**, 187 (1977).
- ⁴³ J. K. Badenhoop and F. Weinhold, *J. Chem. Phys.* **107**, 5422 (1997).
- ⁴⁴ C. J. Cramer and D. G. Truhlar, *J. Am. Chem. Soc.* **113**, 8305 (1991).
- ⁴⁵ G. D. Hawkins, C. J. Cramer, and D. G. Truhlar, *J. Phys. Chem. B* **102**, 3257 (1998). See
Tables included in supporting information.

TABLE I: Solvation free energies (kcal/mol) for selected molecules and ions in water, calculated with this model using a dielectric function $\epsilon = \epsilon(\rho)$ determined by the electron density,^a and $\epsilon = \epsilon(\gamma(\mathbf{R}_I))$ determined by the atomic positions with $\beta=2.4$ (see text). Experimental values^b and results from PCM^c are also shown.

	Expt.	$\epsilon = \epsilon(\rho)$	$\epsilon = \epsilon(\gamma)$	PCM
H ₂ O	-6.3	-8.4	-8.8	-5.4
CH ₃ CONH ₂	-9.7	-10.5	-8.0	-4.6
CH ₃ NH ₃ ⁺	-73	-81.0	-81.9	-65.1
NO ₃ ⁻	-65	-57.8	-60.6	-62.6
Cl ⁻	-75	-66.9	-68.6 ^d	-72.6

^a From reference¹³. ^b From references^{44,45}. ^c Obtained with the Polarizable Continuum Model as implemented in Gaussian 03.^{9,27} ^d The van der Waals radius for ionic chlorine was set equal to

2.059 Å, from reference⁴³.

TABLE II: Adsorption energies for water on the anatase (101) surface in the gas phase and in solution, in both the molecular and dissociative configurations at different coverages. Values are given in kcal per H₂O molecule.

	Molecular		Dissociative	
	$\theta = 0.25$	$\theta = 1$	$\theta = 0.25$	$\theta = 1$
Gas phase	-19.4	-17.8	-1.3	-7.4
Solution	-	-3.0	-	6.6

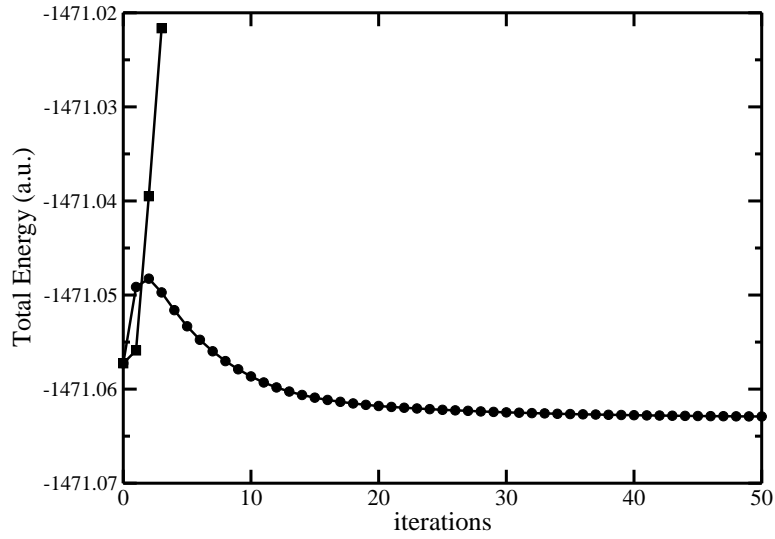


FIG. 1: Total energy during two different Car-Parrinello electronic minimizations in a continuum solvent (the structure is the TiO_2 slab described in section III). The squares indicate the results for a dielectric function depending on the charge density, whereas the circles correspond to the same computational experiment, but removing V_ϵ from the total potential (see text). Both runs used the same calculation parameters and were restarted from the wavefunction converged in vacuum.

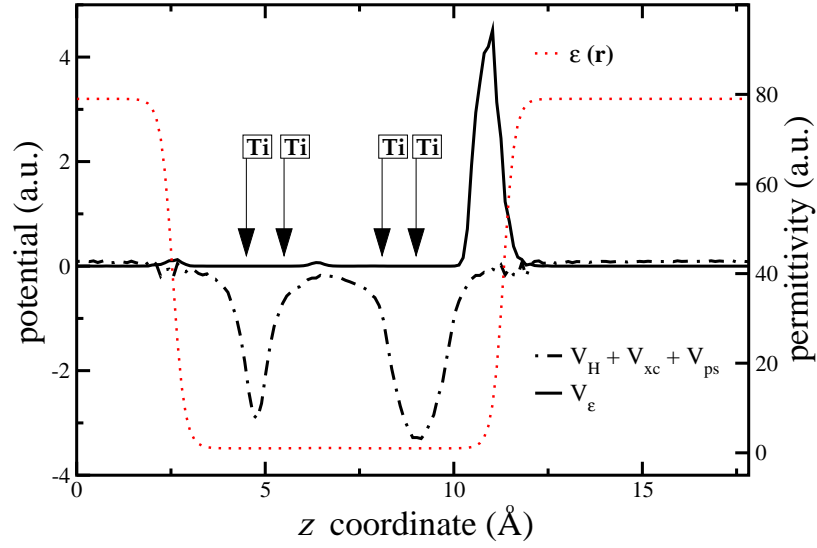


FIG. 2: Variation of V_ϵ and of the effective potential along the z -direction (perpendicular to the slab) at a selected point on the x - y plane, corresponding to the position of one of the exposed Ti atoms of the surface. The dotted line represents the permittivity, referenced on the right axis. The arrows point to the approximate location of each of the titanium layers.

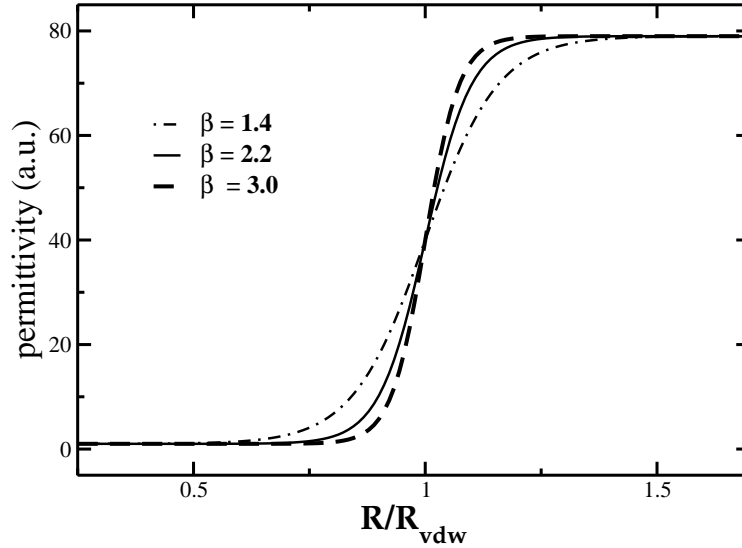


FIG. 3: The permittivity around an oxygen atom as a function of the distance, for different values of the parameter β , according to the position-dependent dielectric defined in Eqs. (9) and (10). The transition, centered around the van der Waals radius, becomes sharper as β is increased.

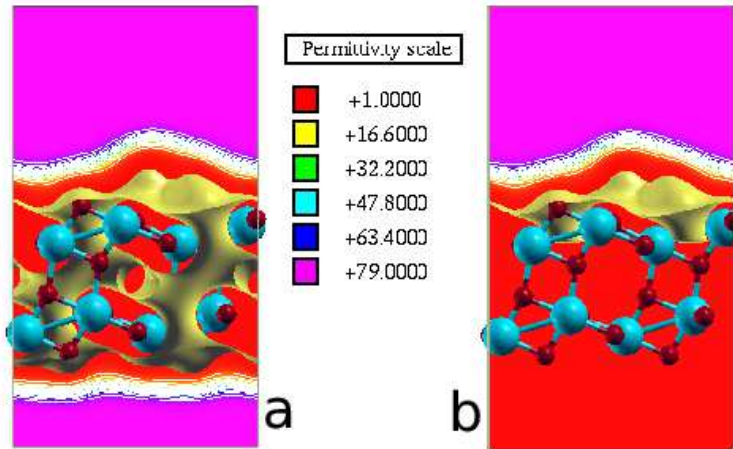


FIG. 4: Contour plot of the dielectric function $\epsilon(\mathbf{r})$ in a supercell containing a four layers slab representing the anatase (101) face of TiO_2 . An isosurface corresponding to $\epsilon(\mathbf{r})=1.4$ is displayed in yellow. In (a) the solvent percolates through the surface, whereas in (b) it is excluded from the slab by virtue of the artifact given in relation (19).

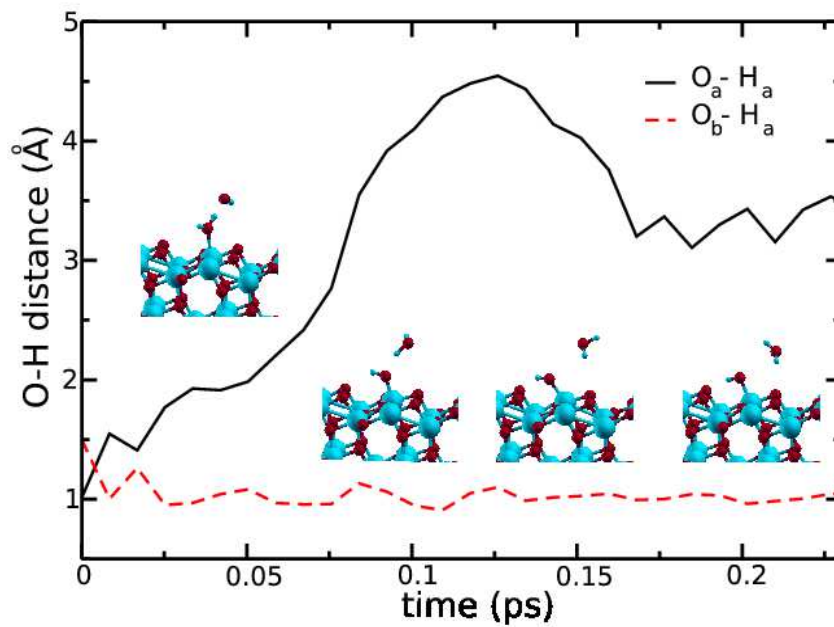


FIG. 5: Interatomic distances O_a-H_a and O_b-H_a during a molecular dynamics simulation of a proton transfer process, from an adsorbed water molecule to a hydroxide ion in a continuum solvent. O_a and O_b are the oxygen atoms of the initially adsorbed water molecule and the hydroxide, respectively, and H_a is the exchanged proton. At the beginning of the simulation the OH^- group is H-bonded to the water molecule. The geometry of the system is shown in the inset for selected time steps.

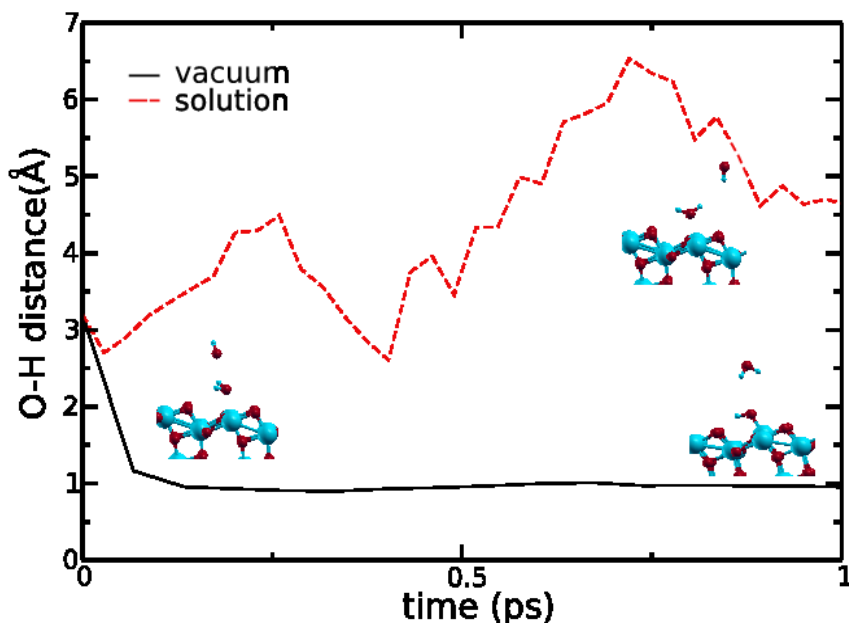


FIG. 6: Interatomic distance O_b-H_a during the molecular dynamics simulations of an adsorbed water molecule in the presence of an hydroxide ion initially situated 4\AA above the surface. O_b is the oxygen atom of the hydroxide and H_a is a proton of the water molecule, which is rapidly exchanged during the gas phase dynamics. The starting geometry is shown on the left, while the upper and lower figures on the right depict the atomic structures after 1 ps of dynamics in vacuum and in solution, respectively.

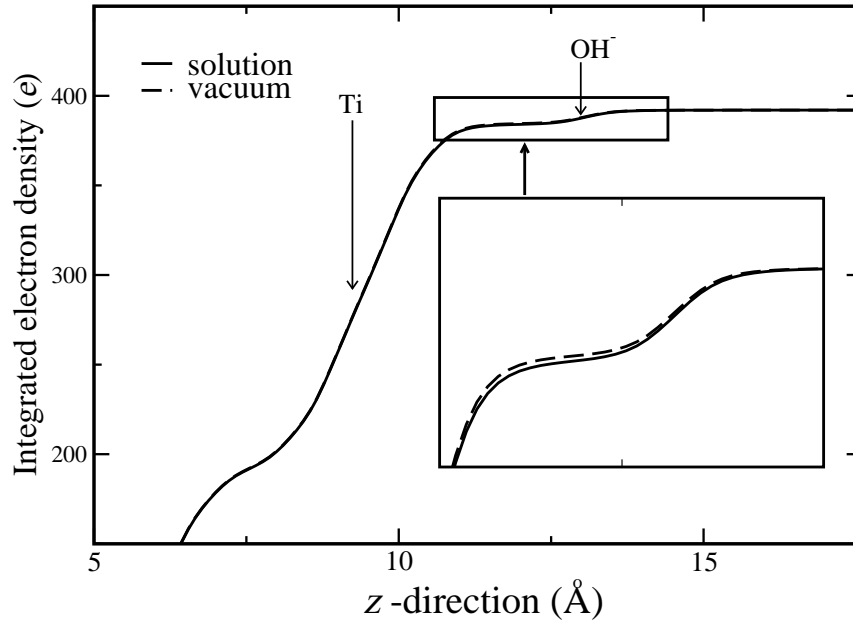


FIG. 7: Electron density integrated on the xy plane, and displayed as a function of the z coordinate, for the hydroxyl anion situated 4\AA above the surface. The approximate positions of the upper Ti layer and of the OH^- ion are indicated with arrows. Enlargement of the interfacial region shows a depletion of the electron density in solution with respect to vacuum. There is an average difference of about $0.5 e$ between the two curves, owing to the stabilization of the electronic charge of the hydroxyl anion surrounded by the dielectric.